Supplementary Information

Supplementary Figure 1

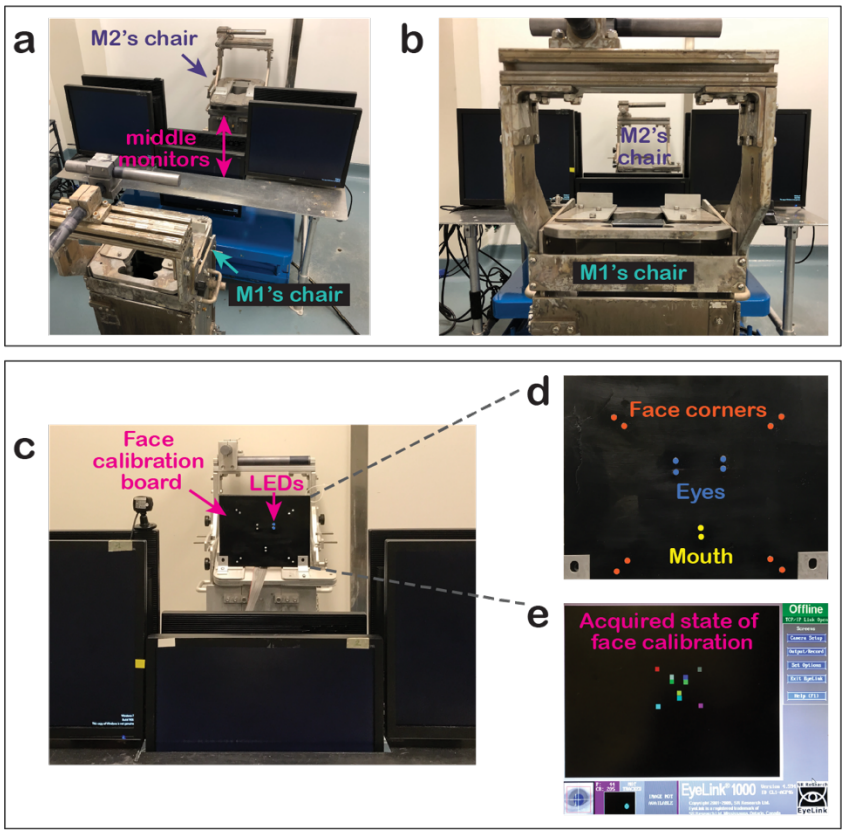

Figure S1. Experimental setup and face calibration board, related to Figure 1. (**a–b**) The experimental setting for live social gaze interaction where a pair of monkeys sat in primate chairs facing each other. The two middle monitors could be lowered down or raised up by using a remote hydraulic system so that the monkeys were able to or not able to see each other. (**c–d**) Customized face calibration LED board for face calibration where LED lights were aligned to a monkey's eyes, mouth, and the four corners of the face. Two sets of LED lights were built to fit two different sizes of monkey faces. The different colors in **d** are only for illustrative purpose. The LED lights always displayed the same color in reality. (**e**) An example state of acquired face calibration, in which each colored square represents an acquired mapping between gaze position and one of the LED positions on the face calibration board.

Supplementary Figure 2

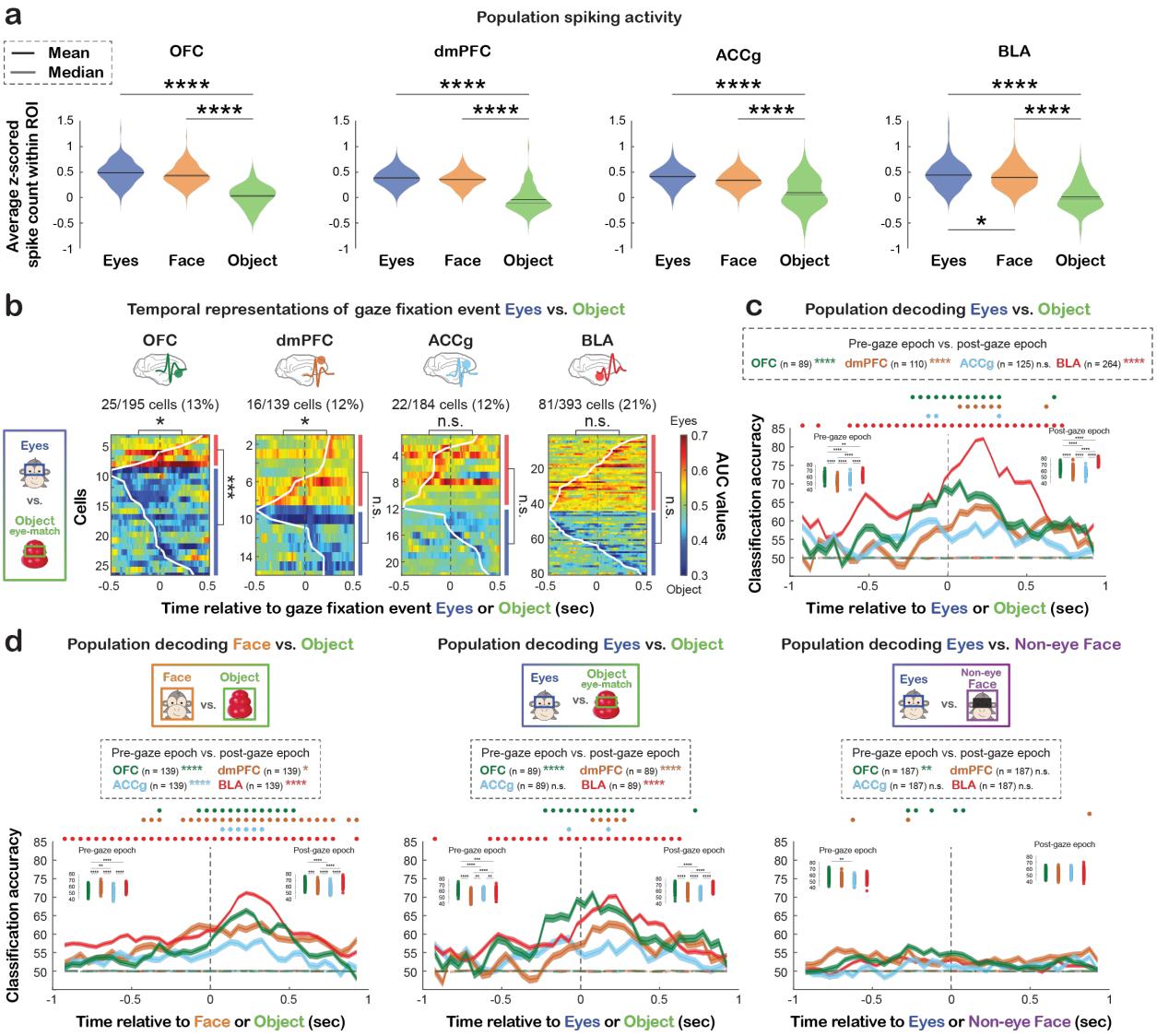

Figure S2. Additional analysis of population spiking activity, temporal representations and population decoding of looking at *Eyes* vs. *Object*, as well as additional analyses of population decoding using matching number of cells across regions, related to Figure 2 and Figure 3. (**a**) Distributions of z-scored spike counts for looking at *Eyes*, *Face*, and *Object*. At the population level, all four brain areas exhibited greater mean activity when looking at *Eyes* and *Face*, compared to *Object* (all $p < 0.0001$, Tukey test), and BLA also showed greater mean activity for *Eyes* than *Face* ($p = 0.04$, Tukey test). * $p < 0.05$, **** $p < 0.0001$, two-way ANOVA, Tukey test. (**b**) Temporal profiles of spiking activity for *Eyes* vs. *Object* with matching ROI sizes. Same format as **Fig. 3a–b**. The data are aligned to the time of gaze fixation event onset with each row representing a cell sorted based on the first bin with significant AUC (white contour). Warm colors indicate greater activity for looking at *Eyes* (AUC > 0.5), whereas cold colors indicate greater activity for *Object* (AUC < 0.5). The asterisks on the top of each heatmap indicate the comparisons of the proportions of cells that began discriminating *Eyes* from *Object* during the pre-gaze epoch vs. post-gaze epoch. To the right of each heatmap, the red bar represents the proportion of cells with

greater activity for *Eyes* and the blue bar for greater activity for *Object*. * $p < 0.05$, *** $p < 0.001$, n.s, not significant, Chi-square test, FDR-corrected. (**c**) Population decoding accuracy for *Eyes* vs. *Object* with matching ROI sizes in OFC (green), dmPFC (brown), ACCg (blue), and BLA (red), same format as **Fig. 3c–d**. Real data are shown in solid lines and empirically derived null data are in dotted lines. Circles at the top indicate the time bins with decoding accuracy significantly higher than the null in corresponding colors ($p < 0.001$, permutation test). For each brain region, asterisks next to the number of cells shown in the box indicate the significance of comparing classification accuracy between the pre-gaze epoch and the post-gaze epoch (Wilcoxon sign rank test, two-sided, FDR-corrected). **** $p < 0.0001$, n.s, not significant. Comparisons of classification accuracy across regions for each time epoch are shown in the inset plots (Wilcoxon rank sum test, two-sided, FDR-corrected). Each data point represents the median classification accuracy of an iteration. ** $p < 0.01$, **** $p < 0.0001$, n.s, not significant. (**d**) Population decoding accuracy for *Face* vs. *Object* with matching ROI size (left, n = 139), *Eyes* vs. *Object* with matching ROI size (middle, n = 89), and *Eyes* vs. *Non-eye Face* (right, n = 187) using matching number of OFC, dmPFC, ACCg, and BLA cells (STAR Methods). Same format as (**c**). * $p < 0.05$, ** $p < 0.01$, *** $p < 0.001$, **** $p < 0.0001$, n.s, not significant.

Supplementary Figure 3

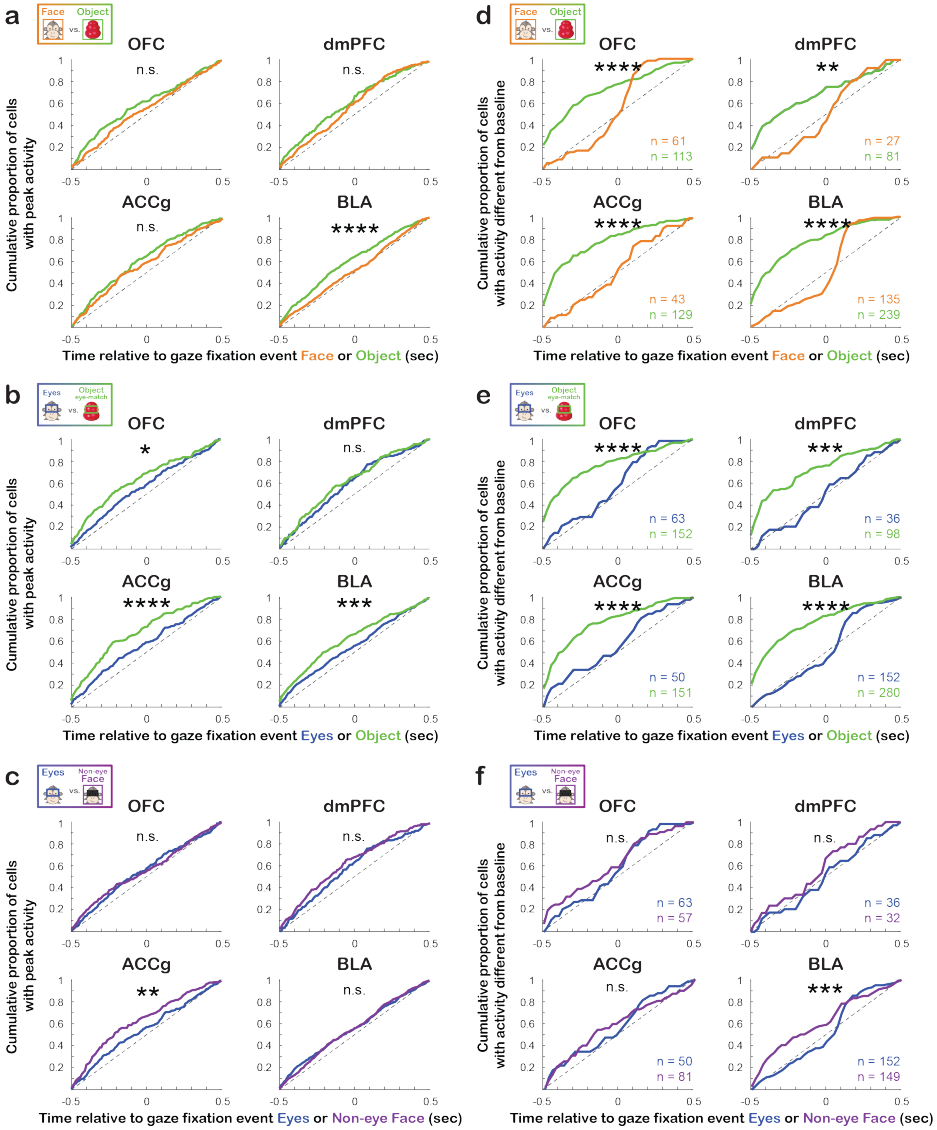

Figure S3. Additional analyses of temporal profiles of spike activity during social gaze fixation events, related to Figure 3. a–c, Cumulative proportions of cells with peak spiking activity that occurred at different time points during the 1-sec period centered on looking at *Face* (orange) and *Object* (green) with matching ROI sizes (**a**), *Eyes* (blue) and *Object* with matching ROI sizes (**b**), as well as *Eyes* and *Non-eye Face* (purple) (**c**). Differences in the cumulative distributions between pairs of ROIs are shown as: * $p < 0.05$, ** $p < 0.01$, *** $p < 0.001$, **** $p < 0.0001$, n.s, not significant, Wilcoxon rank sum test, two-sided. **d–f,** Cumulative proportions of cells that began to show differentiated activity from the baseline at different time points during the 1-sec period centered around looking at *Face* and *Object* with matching ROI sizes (**d**), *Eyes* and *Object* with matching ROI sizes (**e**), and *Eyes* and *Non-eye Face* (**f**). Numbers (n) shown on the plots represent the number of cells involved in this analysis that showed differentiated activity from the baseline within the 1-sec period. Differences in the cumulative distributions between pairs of ROIs are shown as: ** $p < 0.01$, *** $p < 0.001$, **** $p < 0.0001$, n.s, not significant, Wilcoxon rank sum test, two-sided.

Supplementary Figure 4

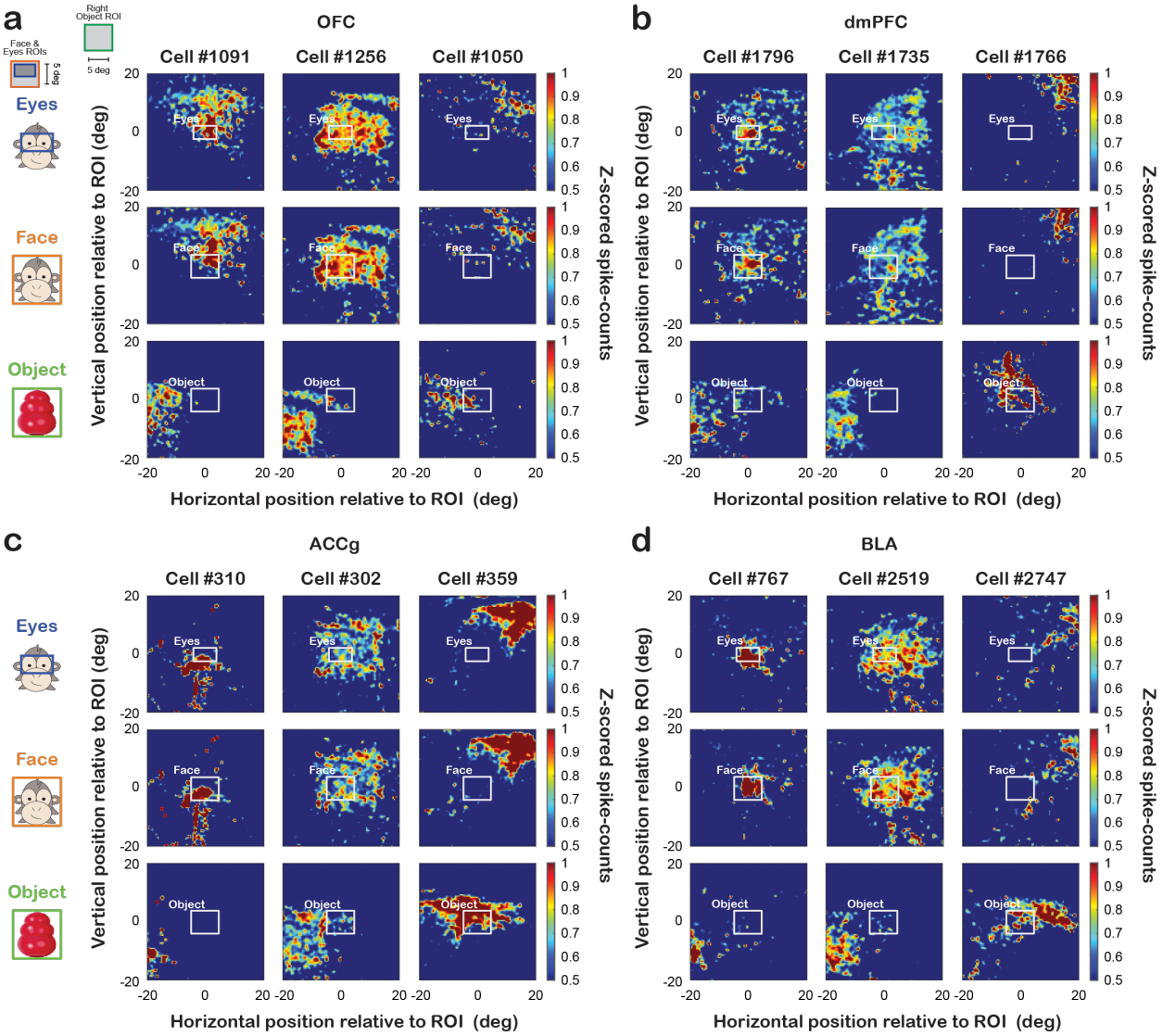

Figure S4. Single-cell examples of spike density maps for *Eyes*, *Face*, and *Object* ROIs, related to Figure 4. (**a–d**), Z-scored spike density heatmaps of three example cells from each brain region, OFC (**a**), dmPFC (**b**), ACCg (**c**), and BLA (**d**), based on recorded monkey's gaze positions relative to the center of partner monkey's *Eyes* (first row), *Face* (second row) and *Object* (last row). Top left inset, the layout of the setup for reference. Some cells increased activity selectively when fixating within *Eyes* or *Face*, but not *Object* (first column), while others did so in a more spatially distributed manner (second column). Another group of cells fired more selectively for fixations closer to *Object* (third column).

Supplementary Figure 5

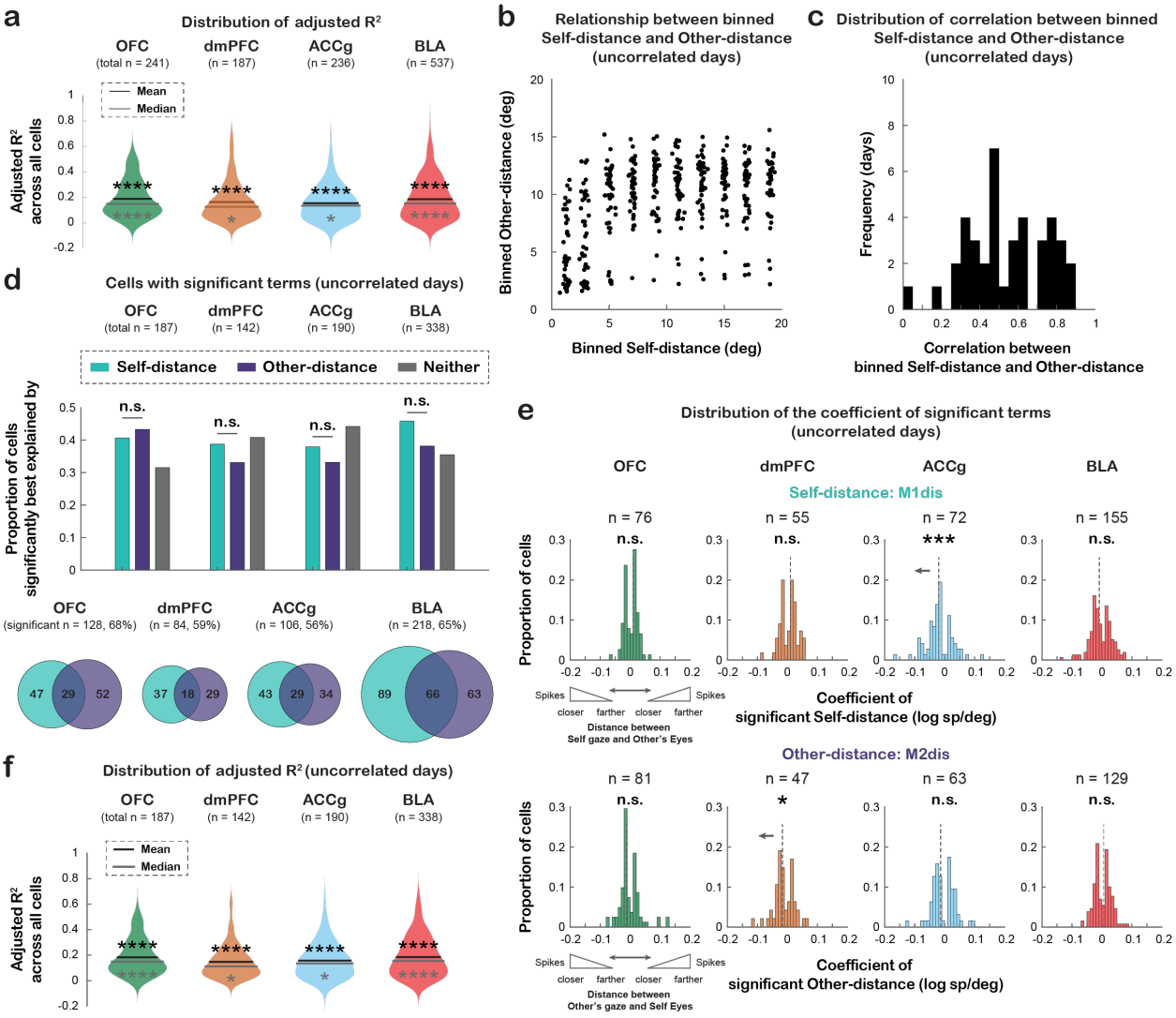

Figure S5. Additional analyses on social gaze monitoring, related to Figure 4. (**a**) Distributions of adjusted R^2 of all cells in each region. The real mean and median adjusted R^2 was compared to the null distribution of mean and median adjusted R^2 for each region (mean shown by black lines, always greater, p = 0 for all regions; median shown by gray lines, p < 0.03 for all regions, permutation test). * p < 0.05, **** p = 0. (**b**) Relationship between binned Self-distance and Other-distance across uncorrelated days (STAR Methods). (**c**) Distribution of correlation between binned Self-distance and Other-distance across uncorrelated days. The median correlation is 0.48. Two-thirds of days (28 out of 42 days) had uncorrelated binned Self-distance and Other-distance. (**d**) Proportions of cells in each region from uncorrelated days whose activity significantly tracked Self-distance (mint), Other-distance (purple), or neither (gray), shown in both bar plots and Venn diagrams. All four areas contained comparable proportions of cells that significantly tracked Self-distance and Other-distance (all $\chi^2 < 3.80$, p > 0.30; Chi-square test, FDR-corrected). Moreover, there was no regional difference in the proportion of cells that significantly tracked Self-distance ($\chi^2 = 4.13$ and p = 0.47, FDR-corrected) or Other-distance ($\chi^2 = 5.46$ and p = 0.42). n.s, not

significant, Chi-square test with FDR correction. (**e**) Distribution of coefficient of neurons from uncorrelated days that significantly tracked Self-distance (top) or Other-distance (bottom). ACCg showed a population bias towards a negative coefficient of Self-distance ($p < 0.001$, Wilcoxon sign-rank test, two-sided), whereas dmPFC showed a bias towards a negative coefficient of Other-distance ($p = 0.03$, Wilcoxon sign-rank test). * $p < 0.05$, *** $p < 0.001$, n.s, not significant, Wilcoxon sign-rank test, two-sided. (**f**) Distributions of adjusted R^2 of all cells in each region from uncorrelated days. The real mean and median adjusted R^2 was compared to the null distribution of mean and median adjusted R^2 for each region (mean shown by black lines, always greater, $p = 0$ for all regions; median shown by gray lines, $p < 0.02$ for all regions, permutation test). * $p < 0.05$, **** $p = 0$.

Supplementary Figure 6

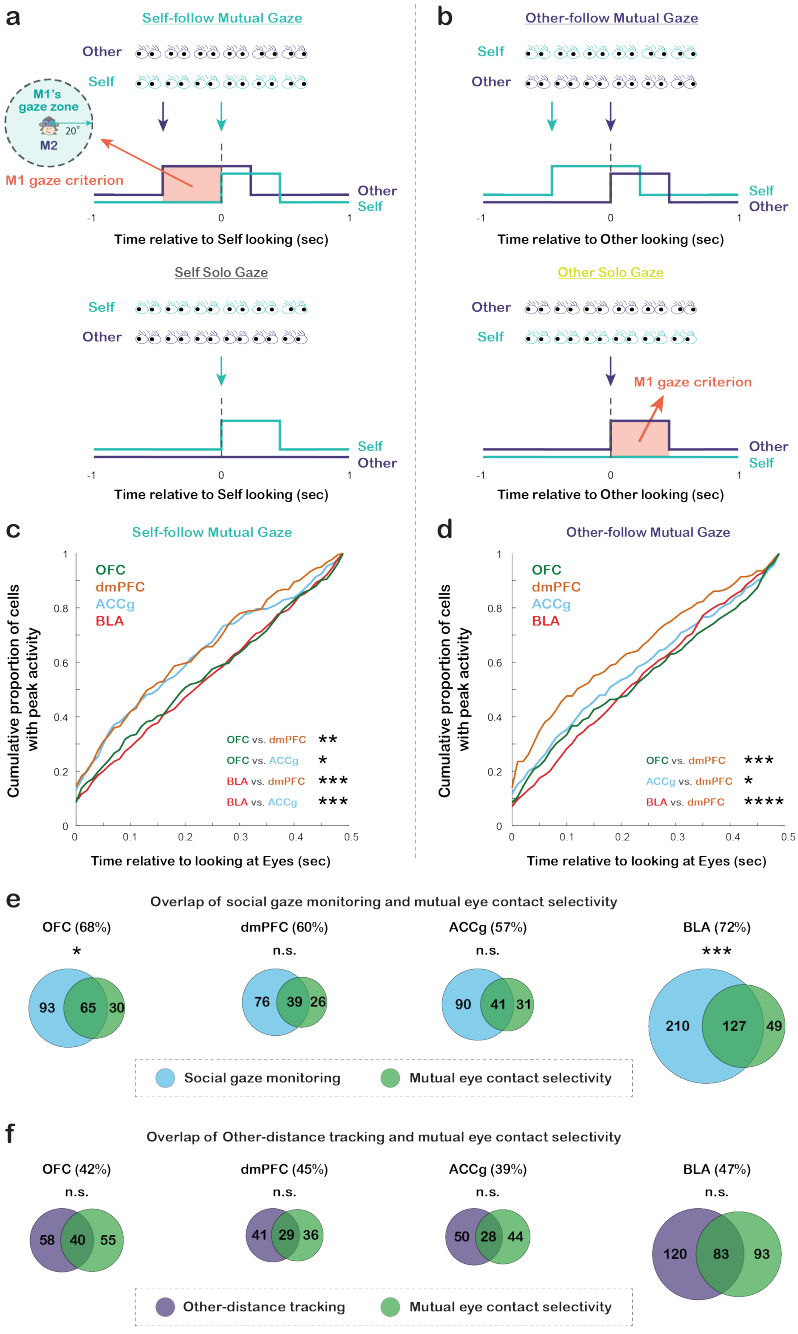

Figure S6. Illustrative diagrams for neural analyses of *Interactive Mutual Gaze* and *Solo Gaze*, temporal profiles of *Interactive Mutual Gaze*, and overlap between neurons involved in social gaze monitoring and mutual eye contact, related to Figure 5 and Figure 6. (**a**) For each cell, spiking activity associated with *Self-follow Mutual Gaze* (top) was compared to *Self Solo Gaze* (bottom), both aligned to the time of M1(self) looking at M2's (other) eyes. (**b**) Similarly, spiking activity associated with *Other-follow Mutual Gaze* (top) was compared to *Other Solo Gaze* (bottom), both aligned to the time of M2 looking at M1's eyes. The time segment marked in orange represents the period to which we applied a gaze criterion for M1 (STAR Methods). (**c**) Cumulative proportion of cells in each brain region that exhibited

peak spiking activity at different time points following the onset of *Self-follow Mutual Gaze* events. OFC and BLA populations showed peak activity later compared to dmPFC and ACCg populations after the onset of *Self-follow Mutual Gaze* events (OFC vs. dmPFC: $p < 0.005$; OFC vs. ACCg: $p = 0.01$; BLA vs. dmPFC: $p < 0.001$; BLA vs. ACCg: $p < 0.001$; both $p > 0.7$ for the other two comparisons, Wilcoxon rank sum test, two-sided). * $p < 0.05$, ** $p < 0.01$, *** $p < 0.001$; Wilcoxon rank sum test, two-sided. (**d**) Cumulative proportion of cells in each brain region that exhibited peak spiking activity at different time points following the onset of *Other-follow Mutual Gaze* events. OFC, ACCg, and BLA populations showed peak activity later compared dmPFC population after the onset of *Other-follow Mutual Gaze* events (OFC vs. dmPFC: $p < 0.001$; ACCg vs. dmPFC: $p = 0.02$; BLA vs. dmPFC: $p < 0.0001$; all $p > 0.11$ for the other comparisons, Wilcoxon rank sum test, two-sided). * $p < 0.05$, *** $p < 0.001$, **** $p < 0.0001$; Wilcoxon rank sum test, two-sided. (**e**) Proportion of cells with mutual eye contact selectivity that were also involved in social gaze monitoring by significantly tracking either Self-distance or Other-distance. These proportions were consistently greater than 50% in all four regions and showed no regional difference ($\chi^2 = 6.88$, $p = 0.13$, Chi-square test, FDR-corrected). Particularly, more than half of cells with mutual eye contact selectivity in OFC and BLA significantly tracked either Self-distance or Other-distance ($\chi^2 = 5.93$, $p = 0.04$, and $\chi^2 = 17.26$, $p < 0.0005$, respectively, Chi-square test compared to 50%, FDR-corrected), whereas about half of cells with mutual eye contact selectivity in dmPFC and ACCg tracked either distance (both $\chi^2 < 0.95$, $p > 0.41$, compared to 50%, FDR-corrected). (**f**) Proportion of cells with mutual eye contact selectivity that also significantly tracked Other-distance specifically. About half of cells with mutual eye contact selectivity in these regions significantly tracked Other-distance (all $\chi^2 < 1.38$, $p > 0.66$, Chi-square test compared to 50%, FDR-corrected), suggesting that many cells that encoded mutual eye contact tracked where partner monkey looked relative to oneself, and there was no regional difference in such proportions ($\chi^2 = 1.62$, $p = 0.67$, FDR-corrected).